

# Deconfined quantum criticality lost

Menghan Song,<sup>1</sup> Jiarui Zhao,<sup>1</sup> Lukas Janssen,<sup>2</sup> Michael M. Scherer,<sup>3</sup> and Zi Yang Meng<sup>1,\*</sup>

<sup>1</sup>*Department of Physics and HKU-UCAS Joint Institute of Theoretical and Computational Physics, The University of Hong Kong, Pokfulam Road, Hong Kong SAR, China*

<sup>2</sup>*Institut für Theoretische Physik and Würzburg-Dresden Cluster of Excellence ct.qmat, TU Dresden, 01062 Dresden, Germany*

<sup>3</sup>*Institute for Theoretical Physics III, Ruhr-University Bochum, D-44801 Bochum, Germany*

(Dated: July 7, 2023)

Over the past two decades, the enigma of the deconfined quantum critical point (DQCP) has never failed to attract broad attention across condensed matter and quantum materials to quantum field theory and high-energy physics communities, as it is expected to offer a new paradigm in theory, experiment, and numerical simulations that goes beyond the Landau-Ginzburg-Wilson framework of symmetry breaking and phase transitions. However, the lattice realizations of DQCP have been controversial. For instance, in the square-lattice spin-1/2  $J$ - $Q$  model, believed to realize the DQCP between Néel and valence bond solid states, conflicting results, such as first-order versus continuous transition, and drifting critical exponents incompatible with conformal bootstrap bounds, have been reported. Here, we solve this two-decades-long mystery by taking a new viewpoint, in that we systematically study the entanglement entropy of square-lattice  $SU(N)$  DQCP spin models, from  $N = 2, 3, 4$  within the  $J$ - $Q$  model to  $N = 5, 6, \dots, 12, 15, 20$  within the  $J_1$ - $J_2$  model. Based on the incremental quantum Monte Carlo algorithm of the entanglement entropy computation, we unambiguously show that for  $N \leq 6$ , the previously determined DQCPs do not belong to unitary conformal fixed points. In contrast, when  $N \geq N_c$  with a finite  $N_c \geq 7$ , the DQCPs correspond to unitary conformal fixed points that can be understood within the Abelian Higgs field theory with  $N$  complex components. From the viewpoint of quantum entanglement, our results suggest the realization of a genuine DQCP between Néel and valence bond solid phases at finite  $N$ , and yet explain why the  $SU(2)$  case is ultimately weakly-first-order, as a consequence of a collision and annihilation of the stable critical fixed point of the  $N$ -component Abelian Higgs field theory with another, bicritical, fixed point, in agreement with four-loop renormalization group calculations. The experimental relevance of our findings is discussed.

*Introduction.*—The famous novel “The Enigma of Arrival” by V. S. Naipaul [1] tells the story of a young Indian from the Caribbean, arriving in post-imperial England, and consciously, over many years, finding himself as a writer. It is the story of a journey, from one place and state of mind to another place and state of mind—from the remote British colony of Trinidad to the ancient countryside of 20th century England—yet the hero has never arrived at a place and state of mind that can be considered as home, both culturally and emotionally. The finding that the old world is lost to gradual but permanent changes is perhaps the enigma of arrival.

The same perplexing state of mind also applies to the investigations of deconfined quantum criticality. Over the past two decades, the enigma of the deconfined quantum critical point (DQCP) has never failed to attract attention across the communities of condensed matter and quantum materials to quantum field theory and high-energy physics. Although the DQCP is believed to offer a new paradigm in theory [2–5], numerical simulations [6–12], and experiments [13–17], going beyond the Landau-Ginzburg-Wilson framework of symmetry breaking and phase transitions, its lattice realizations have remained highly controversial. Take the square-lattice  $SU(2)$   $J$ - $Q$  model [7] as an example: it was initially believed to realize a continuous quantum phase transition between Néel and valence bond solid (VBS) states, but over the years, conflicting results, such as first-order ver-

sus continuous transition [18–24], emergent continuous symmetry with fractionalized excitations [12, 25–27] yet critical exponents incompatible with conformal bootstrap bounds [11, 28, 29], have been reported. No consensus has been reached to date.

Similar complications also occur in many more recent DQCP models, such as the fermionic models realizing sequences of transitions from a Dirac semimetal (DSM) through a quantum spin Hall (QSH) insulator to a superconductor (SC) [9, 30], from a DSM through a VBS to an antiferromagnet (AFM) [10, 31], or from a symmetric DSM through an AFM semimetal to a gapped insulator or superconductor [32]. Although the fermionic models enjoy some advantages over the  $J$ - $Q$  model, e.g., the absence of symmetry-allowed quadruple monopoles and the associated second length scale that corresponds to the breaking of the assumed  $U(1)$  symmetry down to  $\mathbb{Z}_4$ , incompatible critical exponents persist and the accumulating numerical results are also pointing towards the absence of a unitary conformal field theory (CFT) of these DQCPs [9, 10, 30–34].

Overall, after two decades of efforts, the lattice realizations of the DQCP in its original sense of beyond Landau-Ginzburg-Wilson and yet still critical, with emergent continuous symmetry and fractionalized excitations, are still in “The Enigma of Arrival,” and the mystery of their failure of arrival is yet to be explained. In fact, the drift in exponents, their conflicts with conformal boot-

strap bounds, and the seemingly weakly-first-order behavior appear to be a universal phenomenon of the quantum transition between SU(2) and U(1) or  $\mathbb{Z}_4$  breaking phases, pointing towards a common origin.

A possible mechanism that could reconcile the conflicting observations on the DQCP scenario is based on an underlying complex CFT, which is a non-unitary theory at a complex-valued renormalization group (RG) fixed point (FP) [35–37]. Under certain circumstances, such a FP can control the RG flow of a real and unitary physical theory by slowing it down, inducing a large correlation length and pseudo-critical walking behavior, see Fig. 1(c,d). This would be compatible with the observation of a weakly-first-order transition, a large but finite correlation length, seemingly drifting exponents, and it would not be bound by constraints from conformal bootstrap or duality conjectures.

Candidate universal field theories related to the DQCP scenario, which may host such complex CFT behavior, are the  $N$ -component Abelian Higgs (AH) model or the  $CP^{N-1}$  nonlinear sigma model [3, 23, 24, 28, 38]. For example, in the case of the AH model, there is strong evidence for a FP collision [39, 40] at a critical number of complex bosons  $N_c$ . Slightly below  $N_c$ , weakly-first-order behavior occurs, with a correlation length governed by Miransky scaling, i.e., the correlation length becomes exponentially large when approaching  $N_c$  from below. This leads to approximate power laws over orders of magnitude in various observables, however, with slowly drifting exponents, and ultimately a weakly-first-order transition. Similarly, the  $SO(D+2)$ -symmetric nonlinear sigma model with Wess-Zumino-Witten term in  $D$  space-time dimensions has recently been argued to feature a FP annihilation as a function of  $D$  [23, 24].

In fact, such FP collisions have been discussed in a number of other systems, too, including quantum electrodynamics in three space-time dimensions [41–44], many-flavor quantum chromodynamics [35, 44, 45], tensor models [46, 47], Potts models [37, 48], long-range-interacting fermion models [49, 50], and theories with multiple order parameters [51–53]. Although considered a quite general phenomenon in strongly-interacting systems [35], a numerical confirmation has so far proven to be difficult and has not been unambiguously achieved until now beyond simple one-dimensional examples [48]. The basic difficulty arises from the Miransky scaling, which leads to exponentially large correlation lengths at the weakly-first-order transition, preventing a clear distinction between continuous and discontinuous behavior in a finite-size system. Moreover, the underlying FP collision induces a nearly marginal RG direction, tentatively rendering a clean scaling analysis challenging on both sides of the collision.

Therefore, conventional tools to distinguish continuous from discontinuous behavior are fundamentally limited within the complex CFT scenario. In this work, we follow

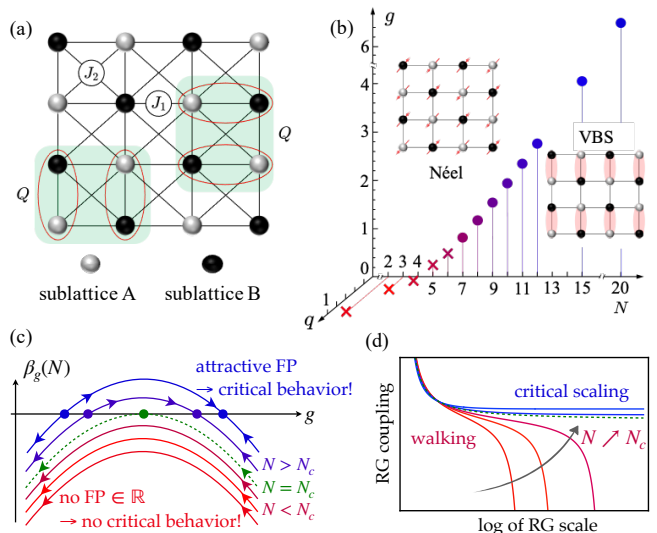


FIG. 1. **SU( $N$ )  $J_1$ - $J_2$ - $Q$  model and its phase diagram.** (a)  $J_1$ - $J_2$ - $Q$  model on square lattice with white (black) sites representing sublattice A (B). Solid lines correspond to nearest-neighbor antiferromagnetic exchange  $J_1$  and next-nearest-neighbor ferromagnetic exchange  $J_2$ . Green shaded squares indicate four-spin ring exchange  $Q$ . (b) Phase diagram as function of  $g = J_2/J_1$ ,  $q = Q/(Q + J_1)$ , and  $N$ . Colored dots and crosses indicate transition points, at which we analyze the finite-size scaling behavior of the EE. When  $N \leq 4$ , the transition is tuned by  $q$  between Néel at small  $Q$  and VBS at large  $Q$ . When  $N > 4$ , the transition is tuned by  $g$  between VBS at small  $J_2$  and Néel at large  $J_2$ . We find the transitions for  $N < 7$  are not compatible with unitary CFTs, showing weakly-first-order transitions denoted by the red-colored crosses. In contrast, those for  $N \geq 7$  are compatible with unitary CFTs and continuous behavior, indicated by the blue-colored dots. (c) Schematic RG  $\beta$  functions and (d) corresponding RG flow trajectories of a representative coupling for different fixed values of  $N$ . For  $N > N_c$ , there are two FPs, shown as blue dots in (c). The attractive one leads to true critical scaling, as indicated by the blue RG trajectories in (d). Decreasing  $N$  shifts the  $\beta$  function down, until the two FPs collide at some critical  $N = N_c$ , indicated by the green dashed curves in (c) and (d). Decreasing  $N$  further, the FPs annihilate and disappear into the complex plane, i.e., no true critical behavior can occur anymore. However, for  $N \lesssim N_c$ , the RG flow remains slow in the vicinity of the now complex FPs, giving rise to walking behavior and drifting in the exponents, see red curves in (c) and (d).

an alternative route to resolve this puzzle numerically, i.e., by analyzing the entanglement entropy (EE).

**Main result.**—Our new viewpoint of FP annihilation and the complex CFT scenario of DQCP is achieved by systematically investigating the scaling of the EE upon partitioning into subregions involving corners [54]. As a proof of concept, we choose the square-lattice SU( $N$ ) DQCP spin model [55–58] from  $N = 2, 3, 4$  (the  $J$ - $Q$  model) to  $N = 5, 6, \dots, 12, 15, 20$  (the  $J_1$ - $J_2$  model), see Fig. 1(a). Using our incremental quantum Monte Carlo (QMC) algorithm to measure the EE [31, 59–64], we un-

ambiguously show that for  $N = 2, 3, 4, 5, 6$ , the previously determined DQCPs all show an EE scaling that is incompatible with unitary CFTs. As a consequence, these DQCPs cannot correspond to continuous transitions and are necessarily weakly-first-order. In contrast, when  $N \geq 7$ , the DQCPs are compatible with unitary CFTs, and are potentially continuous. In fact, in the large- $N$  limit, we show that our numerical results are consistent with the expectations from the AH and nonlinear sigma model descriptions [3, 28, 56, 65]. These field theories feature unitary conformal FPs in the large- $N$  limit [40, 66, 67], which demonstrates the existence of a finite critical  $N_c$ , above which the DQCP becomes continuous. Our numerical results allow us to determine a lower bound for the critical value of  $N$ , namely  $N_c \geq 7$ . This conclusion is further enhanced by observing convergent critical exponents against systems sizes above  $N_c$ , as discussed in the Supplemental Materials [68].

On the field-theory side, estimating the value of  $N_c$  has been a challenging problem over several decades [39, 40, 69]. A four-loop  $\epsilon$  expansion study estimated  $N_c \simeq 12(4)$  [40], while recent simulations of the lattice AH model [70] did not find any evidence for first-order behavior for  $N \geq 10$ , suggesting  $N_c < 10$ . It should be emphasized, however, that higher-loop corrections in the  $\epsilon$  expansion of  $N_c$  are particularly sizable, questioning the validity of the extrapolation to the physical case. On the other hand, it is certainly difficult, if not impossible, in any finite-size computation of conventional local observables, such as magnetization, susceptibility, specific heat, etc., to distinguish a continuous transition from a weakly-first-order transition, which is characterized by a correlation length that significantly exceeds the lattice size.

In our work, we overcome these difficulties by studying the EE, which is a non-local observable and believed to capture the organizing principle of the quantum many-body systems beyond conventional measurements related with order parameters and local responses [61, 71–75]. The log-coefficient of the EE has to satisfy the positivity requirement for a unitary CFT [76]. It allows us to unambiguously demonstrate the absence of a unitary conformal point for  $N < 7$ . Our results prove the realization of a true DQCP between Néel and VBS phases at finite but large  $N$ , and yet explain why the SU(2) case is *not* a true DQCP, but a result of FP annihilation, leading to pseudo-critical behavior and a complex nearby CFT [23, 24, 40]. This explains all the previous difficulties of the violation of the bootstrap bound [29], the drifting of the critical exponents [28], and the indications for weakly-first-order transitions [22, 34], for  $N < 7$ . Such understanding also naturally explains why, experimentally, both in the VBS-AFM DQCP transition in the quantum magnet SrCu<sub>2</sub>(BO<sub>3</sub>)<sub>2</sub> [13–15, 17], and the QSH-SC superconducting quantum criticality in monolayer WTe<sub>2</sub> [77], the systems either exhibit first-order

transitions or intermediate phases, defying the original proposal for an SU(2) DQCP.

*Model and phase diagram.*—We study the SU( $N$ ) spin model defined in a Hilbert space of  $N$  local states (colors) at each site of the square lattice [55–58], as shown in Fig. 1(a). We assume SU( $N$ ) spins in the fundamental representation on sublattice  $A$  and in the conjugate representation on sublattice  $B$ , i.e.,  $|\alpha\rangle_A \rightarrow U_{\alpha,\beta}|\beta\rangle_A$ ,  $|\alpha\rangle_B \rightarrow U_{\alpha,\beta}^*|\beta\rangle_B$ , with the state  $\sum_{\alpha} |\alpha\rangle_A |\alpha\rangle_B$  an SU( $N$ ) singlet [78, 79]. The Hamiltonian reads

$$H = -\frac{J_1}{N} \sum_{\langle ij \rangle} P_{ij} - \frac{J_2}{N} \sum_{\langle\langle ij \rangle\rangle} \Pi_{ij} - \frac{Q}{N} \sum_{\langle i,j \rangle, \langle k,l \rangle} P_{ij} P_{kl}, \quad (1)$$

where the  $J_1$  term is the SU( $N$ ) generalization of the nearest-neighbor antiferromagnetic interaction, as  $P_{ij}$  is defined as the projection operator onto the SU( $N$ ) singlet between a pair of spins  $i$  and  $j$  on different sublattices, and the  $J_2$  term is the SU( $N$ ) generalization of the next-nearest-neighbor ferromagnetic interaction, as  $\Pi_{ij}$  is the permutation operator acting between sites having the same representation on the same sublattice, i.e.,  $\Pi_{ij}|\alpha\beta\rangle = |\beta\alpha\rangle$ . We also add a four-spin ring exchange term  $Q$  for the  $N = 2, 3, 4$  cases, where  $\langle i, j \rangle, \langle k, l \rangle$  are spin pairs located on adjacent corners of a 4-site plaquette, see Fig. 1(a). This term preserves the translational and rotational symmetries of the square lattice, and was found to stabilize a VBS state with  $\mathbb{Z}_4$  symmetry-breaking at large  $Q$  [6, 8, 57]. We simulate Eq. (1) with QMC on lattices with linear sizes of  $L = 24, 36, 48, 60, 72, 84, 96, 108$  and at corresponding inverse temperatures  $\beta = \frac{1}{T} = L$ . We set  $J_1 = 1$  as the energy unit.

The phase diagram of Eq. (1), spanned by the axes of  $q = \frac{Q}{(J_1+Q)}$ ,  $g = J_2/J_1$ , and  $N$ , is shown in Fig. 1(b). It is consistent with previous QMC works [6, 8, 55–58, 80]. At  $N = 2, 3, 4$ , a transition between Néel and VBS state can be induced upon tuning  $q = \frac{Q}{(J_1+Q)}$  for fixed  $J_2 = 0$  [7, 8, 19, 81, 82]. For  $N \geq 5$ , the  $J_1$ -only model for  $J_2 = Q = 0$  already has a VBS ground state [80, 83, 84], and a Néel-VBS transition can be induced by tuning  $g = J_2/J_1$  for fixed  $Q = 0$  [6, 57, 80]. In the Supplemental Material (SM) [68], we show that our critical couplings  $q_c$  and  $g_c$  agree with those in the literature [7, 8, 19, 55–58, 81, 82]. We also determine the corresponding critical exponents at a few representative  $N$ .

*Finite-size scaling of EE.*—The universal CFT data of these transitions in the phase diagram of Fig. 1(b) can be revealed from entanglement measurements [54, 71, 72, 85, 86]. To this end, we have developed an incremental QMC algorithm [31, 59–64, 87] for the SU( $N$ ) spin model. Details of the implementation are given in the SM [68]. Here we only mention that, to compute the second-order Rényi EE for quantum spin systems, there are many previous attempts based on the swap operator and its extensions [75, 88–93] and the data quality is al-

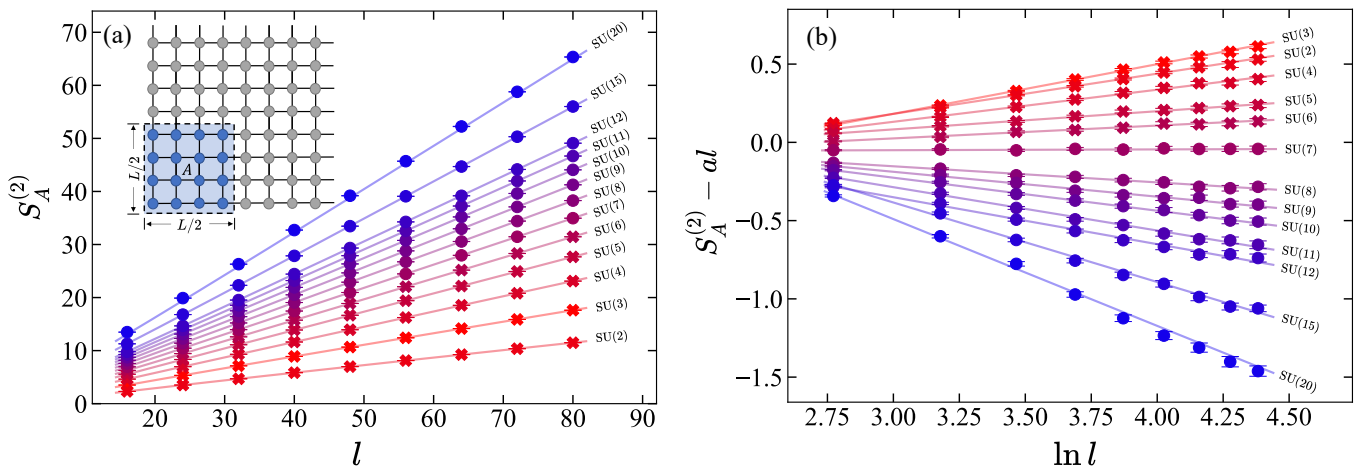


FIG. 2. **Rényi EE and its scaling behavior at the  $SU(N)$  DQCPs.** (a) EE  $S_A^{(2)}$  as function of boundary length  $l = 2L$  of the entanglement region  $A$  for different values of  $N$ , with the partitioning shown in the inset. The area-law behavior  $\propto al$  becomes more prominent for increasing  $N$ . (b) EE with area-law contribution subtracted, i.e.,  $S_A^{(2)} - al$ , as function of  $\ln l$  for different values of  $N$ . The slopes of these curves determine the coefficient  $s$  of the logarithmic term in Eq. (2), with a negative (positive) slope corresponding to a positive (negative) value of  $s$ . One sees that  $s < 0$  for  $N \leq 6$ , implying that the AFM-VBS transition for these values of  $N$  is not described by a unitary CFT. For  $N \geq 7$ , we find  $s \geq 0$ , permitting a unitary CFT description. Curves for  $N \geq 11$  in (b) are offset by a constant for better visualization. Colors of data points for different  $N$  characterize the sign of the log-term coefficient  $s$  with red (blue) represents negative (positive) values.

ways a serious issue when approaching large system sizes for extracting the expected universal scaling coefficients. This problem is completely solved by the incremental algorithm [31, 59–64, 87, 94, 95], which converts the Rényi EE into the free energy difference between partition functions on two different manifolds, with the help of Jarzynski equality [94] and incremental trick. This method makes the precise determination of EE scaling on various 2D quantum spin models possible with exquisite data quality. And controlled results with the expected CFT data have been obtained, including the log-coefficient of the EE inside the Néel phase of the antiferromagnetic Heisenberg model and at its (2+1)D  $O(3)$  quantum critical points, with both short-range and long-range interactions [59–61, 64] and the topological EE inside the  $\mathbb{Z}_2$  topologically ordered Kagome quantum spin liquid [60].

For a quantum critical point of a 2D lattice model, the expected scaling behavior of the EE is [72, 75]

$$S_A^{(2)}(l) = al - s \ln l + c, \quad (2)$$

where  $l$  is the length of the boundary between the entanglement region  $A$  and the environment  $\bar{A}$ ,  $a$  is the coefficient of the area-law term,  $s$  is the universal constant that contains the CFT data and the geometry of the partitioning [71, 72, 86], and  $c$  is another constant such as the topological EE [61, 73, 74, 96]. In this work, we focus on the universal log-coefficient  $s$ . We have four  $90^\circ$  corners of  $A$ , indicated by the blue shaded area in the inset of Fig. 2(a), contributing to  $s$ . For a spectrum of CFTs, the universal value of  $s$  has previously been numerically and/or analytically computed. For example,

$s = 0.239$  for a free (2 + 1)D Dirac CFT realized on the  $\pi$ -flux square lattice with two spin flavors and two Dirac cones in the Brillouin zone, and four  $90^\circ$  corners of  $A$  [31, 97],  $s = 0.0064$  per  $90^\circ$  corner for a single real free boson [54], and  $s = 0.081(4)$  at the (2 + 1)D  $O(3)$  transition between Néel state and paramagnetic state in spin-1/2 square-lattice model with four  $90^\circ$  corners of region  $A$  [60, 61, 64, 98].

*FP collision from entanglement measurements.*—Our QMC-obtained EE for the Hamiltonian in Eq. (1) are shown in Fig. 2. Since the entanglement region  $A$  is of the size  $L/2 \times L/2$ , the boundary length of  $A$  is  $l = 2L$ . We plot  $S_A^{(2)}(l)$  as function of  $l$  for each  $N$  at its corresponding putative DQCP and fit a functional form according to Eq. (2).

As shown in Fig. 2(a), the obtained  $S_A^{(2)}$  for all  $N$  values are dominated by the area-law scaling, i.e., when  $l$  becomes large, a linear term in  $S_A^{(2)}$  manifests. However, a clear difference appears once we subtract the area-law contribution from the data. In Fig. 2(b), we plot  $S_A^{(2)} - al$  versus  $\ln l$ , the slope of these curves reveals the values and, even more importantly, the signs of  $s$  in Eq. (2) for different  $N$ . One sees that for the cases of  $SU(2)$ ,  $SU(3)$ , ...,  $SU(6)$ , we have  $s < 0$ . Only from  $SU(7)$  on, the value of  $s$  becomes non-negative.

The sign of the log-coefficient in the EE contains very important information. First of all, there is a positivity requirement of  $s$  in the EE for a unitary CFT [76], and our observation of negative values here shows that the putative DQCPs for  $SU(2)$ ,  $SU(3)$ ,  $SU(4)$ ,  $SU(5)$ , and



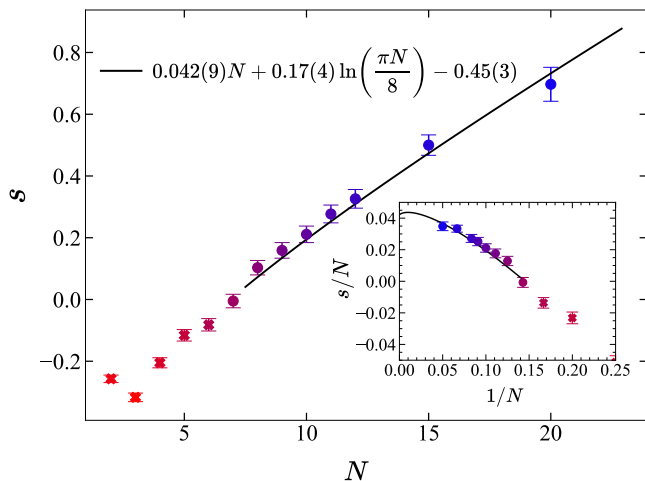


FIG. 3. **Universal corner coefficient in the EE at the  $SU(N)$  DQCP as function of  $N$ .** For  $N \leq 6$ , we find  $s(N) < 0$ , inconsistent with a unitary CFT, while  $s(N) \geq 0$  for  $N \geq 7$ . Solid lines, both in the main panel and the inset, represent a fit of the  $s(N) \geq 0$  data according to Eq. (4), yielding  $a_s = 0.042(9)$ ,  $b_s = 0.17(4)$ , and  $c_s = -0.45(3)$ .

$SU(6)$  are incompatible with this requirement. Exactly the same behavior has been observed in the  $SU(2)$   $J$ - $Q_3$  model [60] and the other spin-1/2 fermion DQCP models [30, 31]. It is interesting to notice that  $s = 0.25(1)$  for our  $SU(2)$   $J$ - $Q$  model matches quantitatively with the previously determined value  $s = 0.25(1)$  for the  $SU(2)$   $J$ - $Q_3$  model with six-spin  $Q_3$  term [60]. These results, combining the observation of the negative log-correction in the EE and disorder operators in the same spin and fermion DQCP models [30, 31, 60, 99], deliver a clear message that all these  $SU(2)$  DQCP models are unanimously incompatible with a unitary CFT description.

However, the teaching of the entanglement in Fig. 2(b) offers more important information than a simple negative verification, as has been obtained in previous works [30, 31, 60, 99]. As  $N$  increases in the  $SU(N)$  model, one sees that the nature of the transition is changing as the slope of  $S_A^{(2)} - al$  versus  $\ln l$  in Fig. 2(b) changes from  $-s \approx 0$  in  $SU(7)$  to  $-s < 0$  from  $SU(8)$  on. We therefore fit the slopes in Fig. 2(b) according to Eq. (2) and plot the obtained  $s$  versus  $N$  in Fig. 3. Here, one sees the DQCPs from  $N \geq 7$  become compatible with a unitary CFT and only from this value of  $N$  on, i.e., for the  $SU(N \geq 7)$  Néel-to-VBS transition, we obtain a true DQCP in the original sense, i.e., a continuous phase transition between two different spontaneously symmetry-breaking phases, described by a unitary CFT.

These results resonate with the four-loop RG calculation of the AH model [40], which suggests that a stable and real FP, describing a continuous Néel-to-VBS transition, exists for  $N \geq N_c = 12(4)$ , but collides with a bicritical FP for  $N \searrow N_c$ . For  $N < N_c$ , the two

FPs annihilate and disappear into the complex plane, leaving behind a weakly-first-order transition, governed by Miransky scaling, characterized by walking behavior and drifting of exponents. This is consistent with the observation of a negative log-coefficient  $s(N) < 0$  for  $N = 2, 3, 4, 5, 6$  seen in the EE measurements within our QMC simulations, implying the absence of true criticality.

*FP collision from large- $N$  limit.*—One question that remains concerns the form of the corner contribution  $s$  as function of  $N$ . To this end, one shall seek help from the large- $N$  critical behavior of our model in Eq. (1), which is expected to be described by the  $CP^{N-1}$  nonlinear sigma model or the  $N$ -component AH model [23, 24, 28, 56–58, 67]. At large  $N$ , the two field theories are believed to realize the same universality class [100, 101]. This expectation can be substantiated using double expansions of critical exponents at both large  $N$  and small  $\epsilon$ , which turn out to agree, up to the orders calculated, order by order with each other in the two models [40]. Computing the corner contribution to the EE scaling in either of these models within, say, a  $1/N$  expansion, is a formidable task, which has not been achieved to date. In standard  $O(N)$  models, the corner contribution has been shown to measure the effective number of degrees of freedom [98, 102], and, in fact, numerical simulations [90, 103] yielded estimates that are not far from the values of the corresponding Gaussian field theories [54]. This has been interpreted to arise from the fact that the  $O(N)$  Wilson-Fisher FP can be reached by perturbing around  $N$  free fields. The behavior of the corner contribution at the  $SU(N)$  DQCP at large  $N$  can be deduced upon assuming that a similar correspondence holds for the AH model. In fact, in a  $(2+1)$ D CFT, a measure of the effective number of degrees of freedom is given by the sphere free energy  $F$  [104], which is defined as the entanglement across a circle [105], and is related to the Euclidean partition function of the CFT on the three-dimensional sphere [106]. The sphere free energy  $F$  of a 3D CFT can also be understood as the three-dimensional generalization of the central charge  $c$  of a 2D CFT [107].

In the AH model, the sphere free energy has the form [105]

$$F(N) = a_F N + b_F \ln\left(\frac{\pi N}{8}\right) + c_F + \mathcal{O}(1/N), \quad (3)$$

where  $a_F = \frac{\ln 2}{4} - \frac{3\zeta(3)}{8\pi^2}$  is twice the value for a free real scalar boson [108],  $b_F = 1/2$ , and  $c_F = -\frac{\zeta(3)}{8\pi^2}$ . In the above equation, the leading term  $\propto a_F$  can be understood as the free-field contribution, the logarithmic term  $\propto b_F$  is the contribution from the  $U(1)$  gauge field, and the constant term  $\propto c_F$  arises from bosonic self-interactions. For the corner contribution to the EE, we thus expect an

analogous form

$$s(N) = a_s N + b_s \ln \left( \frac{\pi N}{8} \right) + c_s + \mathcal{O}(1/N), \quad (4)$$

where  $a_s = 4 \times 2 \times 0.0064 \simeq 0.05$  is the contribution of a single free complex boson at four  $90^\circ$  corners of the sub-region  $A$ . The subleading terms with coefficients  $b_s$  and  $c_s$  are the contributions of the U(1) gauge field and the bosonic self-interactions and have not yet been computed in the literature. Figure 3 shows that our data for  $s(N)$  are indeed consistent with this expectation. From fitting the data between  $N = 8$  and  $N = 20$  to the above form, we obtain

$$a_s = 0.042(9), \quad b_s = 0.17(4), \quad c_s = -0.45(3). \quad (5)$$

Importantly, the leading-order coefficient  $a_s$  agrees with the analytical expectation within the numerical uncertainty. Together with the agreement of the critical exponents with the field-theory expectations (see SM [68]), this is strong evidence that the transition in the SU( $N$ ) lattice model realizes a true DQCP in the large- $N$  limit, described by the  $CP^{N-1}$  nonlinear sigma model or  $N$ -component AH field theory. This demonstrates the existence of a finite universal critical flavor number  $N_c \geq 7$ , at which the stable critical FP of the large- $N$  field theory collides with a bicritical FP, and annihilates with the latter for  $N < N_c$ , leaving behind a runaway flow and a weakly-first-order transition.

*Discussion.*—Our results of a FP collision at  $N_c \geq 7$  and weakly-first-order transitions at  $N = 2, 3, 4, 5, 6$  naturally explain why, experimentally, both in the VBS-AFM transition in the quantum magnet SrCu<sub>2</sub>(BO<sub>3</sub>)<sub>2</sub> [13–15, 17] and the QSH-SC transition in monolayer WTe<sub>2</sub> [77], the systems either exhibit a first-order transition or an intermediate phase, defying the original proposal for the SU(2) DQCP. More recently, a conformal 2D SU(2) DQCP with an SO(5) <sub>$f$</sub>   $\times$  SO(5) <sub>$b$</sub>  global symmetry has been proposed as a description of the cuprate phase diagram with pseudogap metallic,  $d$ -wave superconducting, and charge ordered states as symmetry-breaking phases [109]. Investigating the validity of this proposal using entanglement measurements, as outlined in this work, represents an interesting direction for future research.

At the fundamental level, the scaling violations arising from a FP collision, observed here for the example of the DQCP, has recently been understood as a quite general theme in CFTs [36, 37, 44]. It has been argued that there are three generic mechanisms for the loss of conformality in any number of dimensions [35]: The merging of a FP with the Gaussian FP, the running off of a FP to infinite coupling, and the FP annihilation and complexification mechanism discussed here. The latter scenario has recently been found to be significantly more common than initially anticipated, now being discussed in a number of

situations, ranging from gauge theories in three and four space-time dimensions [39–45, 69] to statistical-physics models [37, 46–48], long-range-interacting fermion models [49, 50], and theories with multiple order parameters [51–53]. Our discovery of the EE as a highly sensitive tool to reveal the intricate phenomena of FP collision and Miransky scaling, characterized by walking behavior and drifting of exponents, now allows the unambiguous identification of whether the FP collision scenarios are indeed realized in the above examples as well.

*Acknowledgments.*—We thank Subir Sachdev, Fakhre Assaad, and Kai Sun for valuable discussions on related topics. MHS, JRZ and ZYM thank Jonathan D’Emidio and Ting-Tung Wang for fruitful discussions on algorithm development and implementation. They acknowledge the support from the Research Grants Council of Hong Kong SAR of China (Grant Nos. 17301420, 17301721, AoE/P-701/20, 17309822), the ANR/RGC Joint Research Scheme sponsored by Research Grants Council of Hong Kong SAR of China and French National Research Agency (Project No. A\_HKU703/22), the K. C. Wong Education Foundation (Grant No. GJTD-2020-01) and the Seed Funding “Quantum-Inspired explainable-AI” at the HKU-TCL Joint Research Centre for Artificial Intelligence. The work of LJ is supported by the Deutsche Forschungsgemeinschaft (DFG) through SFB 1143 (A07, Project No. 247310070), the Würzburg-Dresden Cluster of Excellence *ct.qmat* (EXC 2147, Project No. 390858490), and the Emmy Noether program (JA2306/4-1, Project No. 411750675). MMS acknowledges support from the Deutsche Forschungsgemeinschaft (DFG) through SFB 1238 (C02, Project No. 277146847) and the DFG Heisenberg program (Project No. 452976698). The authors also acknowledge the Tianhe-II platform at the National Supercomputer Center in Guangzhou, the HPC2021 system under the Information Technology Services and the Blackbody HPC system at the Department of Physics, University of Hong Kong, for their technical support and generous allocation of CPU time.

---

\* [zymeng@hku.hk](mailto:zymeng@hku.hk)

- [1] V. S. Naipaul, *The Enigma of Arrival: A Novel in Five Sections* (Viking, 1987).
- [2] T. Senthil, A. Vishwanath, L. Balents, S. Sachdev, and M. P. A. Fisher, Deconfined Quantum Critical Points, *Science* **303**, 1490 (2004).
- [3] T. Senthil, L. Balents, S. Sachdev, A. Vishwanath, and M. P. A. Fisher, Quantum criticality beyond the Landau-Ginzburg-Wilson paradigm, *Phys. Rev. B* **70**, 144407 (2004).
- [4] Y. Q. Qin, Y.-Y. He, Y.-Z. You, Z.-Y. Lu, A. Sen, A. W. Sandvik, C. Xu, and Z. Y. Meng, Duality between the Deconfined Quantum-Critical Point and the Bosonic Topological Transition, *Phys. Rev. X* **7**, 031052 (2017).

- [5] C. Wang, A. Nahum, M. A. Metlitski, C. Xu, and T. Senthil, Deconfined Quantum Critical Points: Symmetries and Dualities, *Phys. Rev. X* **7**, 031051 (2017).
- [6] K. Harada, N. Kawashima, and M. Troyer, Néel and Spin-Peierls Ground States of Two-Dimensional  $SU(N)$  Quantum Antiferromagnets, *Phys. Rev. Lett.* **90**, 117203 (2003).
- [7] A. W. Sandvik, Evidence for Deconfined Quantum Criticality in a Two-Dimensional Heisenberg Model with Four-Spin Interactions, *Phys. Rev. Lett.* **98**, 227202 (2007).
- [8] J. Lou, A. W. Sandvik, and N. Kawashima, Antiferromagnetic to valence-bond-solid transitions in two-dimensional  $SU(N)$  Heisenberg models with multispin interactions, *Phys. Rev. B* **80**, 180414 (2009).
- [9] Y. Liu, Z. Wang, T. Sato, M. Hohenadler, C. Wang, W. Guo, and F. F. Assaad, Superconductivity from the condensation of topological defects in a quantum spin-Hall insulator, *Nat. Commun.* **10**, 1 (2019).
- [10] Y. Da Liao, X. Y. Xu, Z. Y. Meng, and Y. Qi, Dirac fermions with plaquette interactions. I.  $SU(2)$  phase diagram with Gross-Neveu and deconfined quantum criticalities, *Phys. Rev. B* **106**, 075111 (2022).
- [11] H. Shao, W. Guo, and A. W. Sandvik, Quantum criticality with two length scales, *Science* **352**, 213 (2016).
- [12] N. Ma, G.-Y. Sun, Y.-Z. You, C. Xu, A. Vishwanath, A. W. Sandvik, and Z. Y. Meng, Dynamical signature of fractionalization at a deconfined quantum critical point, *Phys. Rev. B* **98**, 174421 (2018).
- [13] J. L. Jiménez, S. P. G. Crone, E. Fogh, M. E. Zayed, R. Lortz, E. Pomjakushina, K. Conder, A. M. Läuchli, L. Weber, S. Wessel, A. Honecker, B. Normand, C. Rüegg, P. Corboz, H. M. Rønnow, and F. Mila, A Quantum Magnetic Analogue to the Critical Point of Water, *Nature* **592**, 370 (2021).
- [14] M. E. Zayed, C. Rüegg, J. Larrea J., A. M. Läuchli, C. Panagopoulos, S. S. Saxena, M. Ellerby, D. F. McMorrow, T. Strässle, S. Klotz, G. Hamel, R. A. Sadykov, V. Pomjakushin, M. Boehm, M. Jiménez-Ruiz, A. Schneidewind, E. Pomjakushina, M. Stingaciu, K. Conder, and H. M. Rønnow, 4-Spin Plaquette Singlet State in the Shastry-Sutherland Compound  $SrCu_2(BO_3)_2$ , *Nat. Phys.* **13**, 962 (2017).
- [15] J. Guo, G. Sun, B. Zhao, L. Wang, W. Hong, V. A. Sidorov, N. Ma, Q. Wu, S. Li, Z. Y. Meng, A. W. Sandvik, and L. Sun, Quantum Phases of  $SrCu_2(BO_3)_2$  from High-Pressure Thermodynamics, *Phys. Rev. Lett.* **124**, 206602 (2020).
- [16] G. Sun, N. Ma, B. Zhao, A. W. Sandvik, and Z. Y. Meng, Emergent  $O(4)$  symmetry at the phase transition from plaquette-singlet to antiferromagnetic order in quasi-two-dimensional quantum magnets, *Chin. Phys. B* **30**, 067505 (2021).
- [17] Y. Cui, L. Liu, H. Lin, K.-H. Wu, W. Hong, X. Liu, C. Li, Z. Hu, N. Xi, S. Li, R. Yu, A. W. Sandvik, and W. Yu, Proximate deconfined quantum critical point in  $SrCu_2(BO_3)_2$ , *Science* **380**, 1179 (2023).
- [18] A. B. Kuklov, M. Matsumoto, N. V. Prokof'ev, B. V. Svistunov, and M. Troyer, Deconfined Criticality: Generic First-Order Transition in the  $SU(2)$  Symmetry Case, *Phys. Rev. Lett.* **101**, 050405 (2008).
- [19] F.-J. Jiang, M. Nyfeler, S. Chandrasekharan, and U.-J. Wiese, From an antiferromagnet to a valence bond solid: evidence for a first-order phase transition, *J. Stat. Mech. Theory Exp.* **2008**, P02009 (2008).
- [20] K. Chen, Y. Huang, Y. Deng, A. B. Kuklov, N. V. Prokof'ev, and B. V. Svistunov, Deconfined Criticality Flow in the Heisenberg Model with Ring-Exchange Interactions, *Phys. Rev. Lett.* **110**, 185701 (2013).
- [21] B. Zhao, J. Takahashi, and A. W. Sandvik, Multicritical Deconfined Quantum Criticality and Lifshitz Point of a Helical Valence-Bond Phase, *Phys. Rev. Lett.* **125**, 257204 (2020).
- [22] J. D'Emidio, A. A. Eberharter, and A. M. Läuchli, Diagnosing weakly first-order phase transitions by coupling to order parameters, [arXiv:2106.15462](https://arxiv.org/abs/2106.15462).
- [23] R. Ma and C. Wang, Theory of deconfined pseudocriticality, *Phys. Rev. B* **102**, 020407 (2020).
- [24] A. Nahum, Note on Wess-Zumino-Witten models and quasiuniversality in  $2+1$  dimensions, *Phys. Rev. B* **102**, 201116 (2020).
- [25] A. Nahum, P. Serna, J. T. Chalker, M. Ortuño, and A. M. Somoza, Emergent  $SO(5)$  Symmetry at the Néel to Valence-Bond-Solid Transition, *Phys. Rev. Lett.* **115**, 267203 (2015).
- [26] N. Ma, Y.-Z. You, and Z. Y. Meng, Role of Noether's Theorem at the Deconfined Quantum Critical Point, *Phys. Rev. Lett.* **122**, 175701 (2019).
- [27] G. J. Sreejith, S. Powell, and A. Nahum, Emergent  $SO(5)$  Symmetry at the Columnar Ordering Transition in the Classical Cubic Dimer Model, *Phys. Rev. Lett.* **122**, 080601 (2019).
- [28] A. Nahum, J. T. Chalker, P. Serna, M. Ortuño, and A. M. Somoza, Deconfined Quantum Criticality, Scaling Violations, and Classical Loop Models, *Phys. Rev. X* **5**, 041048 (2015).
- [29] Y. Nakayama and T. Ohtsuki, Necessary Condition for Emergent Symmetry from the Conformal Bootstrap, *Phys. Rev. Lett.* **117**, 131601 (2016).
- [30] Z. H. Liu, W. Jiang, B.-B. Chen, J. Rong, M. Cheng, K. Sun, Z. Y. Meng, and F. F. Assaad, Fermion Disorder Operator at Gross-Neveu and Deconfined Quantum Criticalities, *Phys. Rev. Lett.* **130**, 266501 (2023).
- [31] Y. Da Liao, G. Pan, W. Jiang, Y. Qi, and Z. Y. Meng, The teaching from entanglement: 2D  $SU(2)$  antiferromagnet to valence bond solid deconfined quantum critical points are not conformal, [arXiv:2302.11742](https://arxiv.org/abs/2302.11742).
- [32] Z. H. Liu, M. Vojta, F. F. Assaad, and L. Janssen, Metallic and Deconfined Quantum Criticality in Dirac Systems, *Phys. Rev. Lett.* **128**, 087201 (2022).
- [33] Z. Wang, Y. Liu, T. Sato, M. Hohenadler, C. Wang, W. Guo, and F. F. Assaad, Doping-Induced Quantum Spin Hall Insulator to Superconductor Transition, *Phys. Rev. Lett.* **126**, 205701 (2021).
- [34] Z. Wang, M. P. Zaletel, R. S. K. Mong, and F. F. Assaad, Phases of the  $(2+1)$  Dimensional  $SO(5)$  Nonlinear Sigma Model with Topological Term, *Phys. Rev. Lett.* **126**, 045701 (2021).
- [35] D. B. Kaplan, J.-W. Lee, D. T. Son, and M. A. Stephanov, Conformality lost, *Phys. Rev. D* **80**, 125005 (2009).
- [36] V. Gorbenko, S. Rychkov, and B. Zan, Walking, weak first-order transitions, and complex CFTs, *J. High Energy Phys.* **10** (2018) 108.
- [37] V. Gorbenko, S. Rychkov, and B. Zan, Walking, Weak first-order transitions, and Complex CFTs II. Two-dimensional Potts model at  $Q > 4$ , *SciPost Phys.* **5**, 050 (2018).

- [38] T. Senthil, Deconfined quantum critical points: a review, [arXiv:2306.12638](https://arxiv.org/abs/2306.12638).
- [39] B. I. Halperin, T. C. Lubensky, and S.-k. Ma, First-Order Phase Transitions in Superconductors and Smectic-A Liquid Crystals, *Phys. Rev. Lett.* **32**, 292 (1974).
- [40] B. Ihrig, N. Zerf, P. Marquard, I. F. Herbut, and M. M. Scherer, Abelian Higgs model at four loops, fixed-point collision, and deconfined criticality, *Phys. Rev. B* **100**, 134507 (2019).
- [41] J. Braun, H. Gies, L. Janssen, and D. Roscher, Phase structure of many-flavor QED<sub>3</sub>, *Phys. Rev. D* **90**, 036002 (2014).
- [42] L. Janssen, Spontaneous breaking of Lorentz symmetry in  $(2 + \epsilon)$ -dimensional QED, *Phys. Rev. D* **94**, 094013 (2016).
- [43] I. F. Herbut, Chiral symmetry breaking in three-dimensional quantum electrodynamics as fixed point annihilation, *Phys. Rev. D* **94**, 025036 (2016).
- [44] S. Gukov, RG flows and bifurcations, *Nucl. Phys. B* **919**, 583 (2017).
- [45] H. Gies and J. Jaeckel, Chiral phase structure of QCD with many flavors, *Eur. Phys. J. C* **46**, 433 (2006).
- [46] I. F. Herbut and L. Janssen, Critical  $O(2)$  and  $O(3)$   $\varphi^4$  theories near six dimensions, *Phys. Rev. D* **93**, 085005 (2016).
- [47] J. A. Gracey, I. F. Herbut, and D. Roscher, Tensor  $O(N)$  model near six dimensions: Fixed points and conformal windows from four loops, *Phys. Rev. D* **98**, 096014 (2018).
- [48] H. Ma and Y.-C. He, Shadow of complex fixed point: Approximate conformality of  $Q > 4$  Potts model, *Phys. Rev. B* **99**, 195130 (2019).
- [49] I. F. Herbut and L. Janssen, Topological Mott Insulator in Three-Dimensional Systems with Quadratic Band Touching, *Phys. Rev. Lett.* **113**, 106401 (2014).
- [50] L. Janssen and I. F. Herbut, Phase diagram of electronic systems with quadratic Fermi nodes in  $2 < d < 4$ :  $2 + \epsilon$  expansion,  $4 - \epsilon$  expansion, and functional renormalization group, *Phys. Rev. B* **95**, 075101 (2017).
- [51] F. Gehring, H. Gies, and L. Janssen, Fixed-point structure of low-dimensional relativistic fermion field theories: Universality classes and emergent symmetry, *Phys. Rev. D* **92**, 085046 (2015).
- [52] I. F. Herbut and M. M. Scherer,  $SO(4)$  multicriticality of two-dimensional Dirac fermions, *Phys. Rev. B* **106**, 115136 (2022).
- [53] K. Ladovrechis, S. Ray, T. Meng, and L. Janssen, Gross-Neveu-Heisenberg criticality from  $2 + \epsilon$  expansion, *Phys. Rev. B* **107**, 035151 (2023).
- [54] H. Casini and M. Huerta, Universal terms for the entanglement entropy in  $2+1$  dimensions, *Nucl. Phys. B* **764**, 183 (2007).
- [55] R. K. Kaul, Quantum phase transitions in bilayer  $SU(N)$  antiferromagnets, *Phys. Rev. B* **85**, 180411 (2012).
- [56] R. K. Kaul, R. G. Melko, and A. W. Sandvik, Bridging Lattice-Scale Physics and Continuum Field Theory with Quantum Monte Carlo Simulations, *Annu. Rev. Condens. Matter Phys.* **4**, 179 (2013).
- [57] R. K. Kaul and A. W. Sandvik, Lattice Model for the  $SU(N)$  Néel to Valence-Bond Solid Quantum Phase Transition at Large  $N$ , *Phys. Rev. Lett.* **108**, 137201 (2012).
- [58] M. S. Block, R. G. Melko, and R. K. Kaul, Fate of  $\mathbb{C}P^{N-1}$  Fixed Points with  $q$  Monopoles, *Phys. Rev. Lett.* **111**, 137202 (2013).
- [59] J. D’Emidio, Entanglement Entropy from Nonequilibrium Work, *Phys. Rev. Lett.* **124**, 110602 (2020).
- [60] J. Zhao, Y.-C. Wang, Z. Yan, M. Cheng, and Z. Y. Meng, Scaling of Entanglement Entropy at Deconfined Quantum Criticality, *Phys. Rev. Lett.* **128**, 010601 (2022).
- [61] J. Zhao, B.-B. Chen, Y.-C. Wang, Z. Yan, M. Cheng, and Z. Y. Meng, Measuring Rényi entanglement entropy with high efficiency and precision in quantum Monte Carlo simulations, *npj Quantum Mater.* **7**, 1 (2022).
- [62] J. D’Emidio, R. Orus, N. Laflorencie, and F. de Juan, Universal features of entanglement entropy in the honeycomb Hubbard model, [arXiv:2211.04334](https://arxiv.org/abs/2211.04334).
- [63] G. Pan, Y. Da Liao, W. Jiang, J. D’Emidio, Y. Qi, and Z. Y. Meng, Computing entanglement entropy of interacting fermions with quantum Monte Carlo: Why we failed and how to get it right, [arXiv:2303.14326](https://arxiv.org/abs/2303.14326).
- [64] M. Song, J. Zhao, Y. Qi, J. Rong, and Z. Y. Meng, Quantum criticality and entanglement for 2d long-range Heisenberg bilayer, [arXiv:2306.05465](https://arxiv.org/abs/2306.05465).
- [65] S. Sachdev, Quantum magnetism and criticality, *Nat. Phys.* **4**, 173 (2008).
- [66] V. Y. Irkhin, A. A. Katanin, and M. I. Katsnelson,  $1/N$  expansion for critical exponents of magnetic phase transitions in the  $CP^{N-1}$  model for  $2 < d < 4$ , *Phys. Rev. B* **54**, 11953 (1996).
- [67] R. K. Kaul and S. Sachdev, Quantum criticality of  $U(1)$  gauge theories with fermionic and bosonic matter in two spatial dimensions, *Phys. Rev. B* **77**, 155105 (2008).
- [68] The QMC implementation of the  $SU(N)$  spin model, the incremental algorithm for the entanglement entropy computation, and representative QMC data of the  $SU(N)$  DQCP points with their critical exponents are shown in the Supplementary Materials.
- [69] I. F. Herbut and Z. Tešanović, Herbut and Tešanović Reply, *Phys. Rev. Lett.* **78**, 980 (1997).
- [70] C. Bonati, A. Pelissetto, and E. Vicari, Lattice Abelian-Higgs model with noncompact gauge fields, *Phys. Rev. B* **103**, 085104 (2021).
- [71] P. Calabrese and J. Cardy, Entanglement entropy and quantum field theory, *J. Stat. Mech. Theory Exp.* **2004**, P06002 (2004).
- [72] E. Fradkin and J. E. Moore, Entanglement Entropy of 2D Conformal Quantum Critical Points: Hearing the Shape of a Quantum Drum, *Phys. Rev. Lett.* **97**, 050404 (2006).
- [73] M. Levin and X.-G. Wen, Detecting Topological Order in a Ground State Wave Function, *Phys. Rev. Lett.* **96**, 110405 (2006).
- [74] A. Kitaev and J. Preskill, Topological Entanglement Entropy, *Phys. Rev. Lett.* **96**, 110404 (2006).
- [75] N. Laflorencie, Quantum entanglement in condensed matter systems, *Phys. Rep.* **646**, 1 (2016).
- [76] H. Casini and M. Huerta, Positivity, entanglement entropy, and minimal surfaces, *J. High Energy Phys.* (2012) 87.
- [77] T. Song, Y. Jia, G. Yu, Y. Tang, P. Wang, R. Singha, X. Gui, A. J. Uzan, M. Onyszczak, K. Watanabe, T. Taniguchi, R. J. Cava, L. M. Schoop, N. P. Ong, and S. Wu, Unconventional Superconducting Quantum Criticality in Monolayer WTe<sub>2</sub>, [arXiv:2303.06540](https://arxiv.org/abs/2303.06540).



- [78] I. Affleck, Large- $n$  Limit of  $SU(n)$  Quantum "Spin" Chains, *Phys. Rev. Lett.* **54**, 966 (1985).
- [79] N. Read and S. Sachdev, Valence-bond and spin-Peierls ground states of low-dimensional quantum antiferromagnets, *Phys. Rev. Lett.* **62**, 1694 (1989).
- [80] K. S. D. Beach, F. Alet, M. Mambrini, and S. Capponi,  $SU(N)$  Heisenberg model on the square lattice: A continuous- $N$  quantum Monte Carlo study, *Phys. Rev. B* **80**, 184401 (2009).
- [81] R. G. Melko and R. K. Kaul, Scaling in the Fan of an Unconventional Quantum Critical Point, *Phys. Rev. Lett.* **100**, 017203 (2008).
- [82] R. K. Kaul, Quantum criticality in  $SU(3)$  and  $SU(4)$  antiferromagnets, *Phys. Rev. B* **84**, 054407 (2011).
- [83] N. Read and S. Sachdev, Large- $N$  expansion for frustrated quantum antiferromagnets, *Phys. Rev. Lett.* **66**, 1773 (1991).
- [84] F. F. Assaad, Phase diagram of the half-filled two-dimensional  $SU(N)$  Hubbard-Heisenberg model: A quantum Monte Carlo study, *Phys. Rev. B* **71**, 075103 (2005).
- [85] H. Casini and M. Huerta, Universal terms for the entanglement entropy in  $2+1$  dimensions, *Nucl. Phys. B* **764**, 183 (2007).
- [86] J. L. Cardy and I. Peschel, Finite-size dependence of the free energy in two-dimensional critical systems, *Nucl. Phys. B* **300**, 377 (1988).
- [87] V. Alba, Out-of-equilibrium protocol for Rényi entropies via the Jarzynski equality, *Phys. Rev. E* **95**, 062132 (2017).
- [88] A. B. Kallin, M. B. Hastings, R. G. Melko, and R. R. P. Singh, Anomalies in the entanglement properties of the square-lattice Heisenberg model, *Phys. Rev. B* **84**, 165134 (2011).
- [89] M. B. Hastings, I. González, A. B. Kallin, and R. G. Melko, Measuring Renyi Entanglement Entropy in Quantum Monte Carlo Simulations, *Phys. Rev. Lett.* **104**, 157201 (2010).
- [90] S. Humeniuk and T. Roscilde, Quantum Monte Carlo calculation of entanglement Rényi entropies for generic quantum systems, *Phys. Rev. B* **86**, 235116 (2012).
- [91] J. Helmes and S. Wessel, Entanglement entropy scaling in the bilayer Heisenberg spin system, *Phys. Rev. B* **89**, 245120 (2014).
- [92] B. Kulchitskiy, C. M. Herdman, S. Inglis, and R. G. Melko, Detecting Goldstone modes with entanglement entropy, *Phys. Rev. B* **92**, 115146 (2015).
- [93] S. V. Isakov, M. B. Hastings, and R. G. Melko, Topological entanglement entropy of a Bose-Hubbard spin liquid, *Nat. Phys.* **7**, 772 (2011).
- [94] C. Jarzynski, Nonequilibrium Equality for Free Energy Differences, *Phys. Rev. Lett.* **78**, 2690 (1997).
- [95] R. W. Zwanzig, High-Temperature Equation of State by a Perturbation Method. I. Nonpolar Gases, *J. Chem. Phys.* **22**, 1420 (1954).
- [96] B.-B. Chen, H.-H. Tu, Z. Y. Meng, and M. Cheng, Topological disorder parameter: A many-body invariant to characterize gapped quantum phases, *Phys. Rev. B* **106**, 094415 (2022).
- [97] J. Helmes, L. E. Hayward Sierens, A. Chandran, W. Witczak-Krempa, and R. G. Melko, Universal corner entanglement of Dirac fermions and gapless bosons from the continuum to the lattice, *Phys. Rev. B* **94**, 125142 (2016).
- [98] A. B. Kallin, E. M. Stoudenmire, P. Fendley, R. R. P. Singh, and R. G. Melko, Corner contribution to the entanglement entropy of an  $O(3)$  quantum critical point in  $2 + 1$  dimensions, *J. Stat. Mech. Theory Exp.* **2014**, P06009 (2014).
- [99] Y.-C. Wang, M. Cheng, and Z. Y. Meng, Scaling of the disorder operator at  $(2 + 1)d$   $U(1)$  quantum criticality, *Phys. Rev. B* **104**, L081109 (2021).
- [100] S. Hikami, Renormalization Group Functions of  $CP^{N-1}$  Nonlinear Sigma Model and  $N$  Component Scalar QED Model, *Prog. Theor. Phys.* **62**, 226 (1979).
- [101] J. March-Russell, On the possibility of second-order phase transitions in spontaneously broken gauge theories, *Phys. Lett. B* **296**, 364 (1992).
- [102] A. B. Kallin, K. Hyatt, R. R. P. Singh, and R. G. Melko, Entanglement at a Two-Dimensional Quantum Critical Point: A Numerical Linked-Cluster Expansion Study, *Phys. Rev. Lett.* **110**, 135702 (2013).
- [103] R. R. P. Singh, R. G. Melko, and J. Oitmaa, Thermodynamic singularities in the entanglement entropy at a two-dimensional quantum critical point, *Phys. Rev. B* **86**, 075106 (2012).
- [104] H. Liu and M. Mezei, A refinement of entanglement entropy and the number of degrees of freedom, *J. High Energy Phys.* **4** (2013) 162.
- [105] I. R. Klebanov, S. S. Pufu, S. Sachdev, and B. R. Safdi, Entanglement entropy of 3-d conformal gauge theories with many flavors, *J. High Energy Phys.* **5** (2012) 36.
- [106] H. Casini, M. Huerta, and R. C. Myers, Towards a derivation of holographic entanglement entropy, *J. High Energy Phys.* **5** (2011) 36.
- [107] S. Giombi and I. R. Klebanov, Interpolating between  $a$  and  $F$ , *J. High Energy Phys.* **3** (2015) 117.
- [108] I. R. Klebanov, S. S. Pufu, and B. R. Safdi, F-theorem without supersymmetry, *J. High Energy Phys.* **10** (2011) 38.
- [109] M. Christos, Z.-X. Luo, H. Shackleton, Y.-H. Zhang, M. S. Scheurer, and S. Sachdev, A model of d-wave superconductivity, antiferromagnetism, and charge order on the square lattice, *Proc. Natl. Acad. Sci.* **120**, e2302701120 (2023).
- [110] K. Harada, T. Suzuki, T. Okubo, H. Matsuo, J. Lou, H. Watanabe, S. Todo, and N. Kawashima, Possibility of deconfined criticality in  $SU(N)$  Heisenberg models at small  $N$ , *Phys. Rev. B* **88**, 220408 (2013).
- [111] J. D'Emidio, M. S. Block, and R. K. Kaul, Rényi entanglement entropy of critical  $SU(N)$  spin chains, *Phys. Rev. B* **92**, 054411 (2015).
- [112] A. W. Sandvik and H. G. Evertz, Loop updates for variational and projector quantum Monte Carlo simulations in the valence-bond basis, *Phys. Rev. B* **82**, 024407 (2010).
- [113] T.-T. Wang and Z. Y. Meng, Emus live on the Gross-Neveu-Yukawa archipelago, [arXiv:2304.00034](https://arxiv.org/abs/2304.00034).
- [114] Z. Yan, X. Ran, Y.-C. Wang, R. Samajdar, J. Rong, S. Sachdev, Y. Qi, and Z. Y. Meng, Fully packed quantum loop model on the triangular lattice: Hidden vison plaquette phase and cubic phase transitions, [arXiv:2205.04472](https://arxiv.org/abs/2205.04472).

# SUPPLEMENTARY MATERIAL FOR “DE- CONFINED QUANTUM CRITICALITY LOST”

## I. SSE IMPLEMENTATION OF SU(N) MODEL

QMC simulations for SU(N) spin model are generalizations of the SU(2) cases [6, 57, 59, 80, 82, 110, 111]. In particular, there are  $N$  colors for spins and loops in the loop-algorithm [112]. Since all the off-diagonal elements in the Hamiltonian Eq. (1) in the main text are negative, Eq. (1) is free of sign-problem if off-diagonal operators appear even number of times along the imaginary time, same as the SU(2) case.

Note that in Eq. (1), the projection operator  $P_{ij}$  only acts between spins belonging to different sublattices (a generalization of nearest-neighbor antiferromagnetic interaction in SU(2) case). In contrast,  $\Pi_{ij}$  only acts between spins belonging to the same sublattice (a generalization of next-nearest neighbor ferromagnetic interaction in SU(2) cases). One can decompose  $P_{ij}$  and  $\Pi_{ij}$  into diagonal and off-diagonal parts, namely  $P_{ij} = P_{ij}^1 - P_{ij}^2$  and  $\Pi_{ij} = \Pi_{ij}^1 - \Pi_{ij}^2$  where 1,2 labels diagonal and off-diagonal parts, respectively. Therefore, all the non-zero matrix elements can be explicitly computed as  $\langle \alpha_A \alpha_B | P_{ij}^1 | \alpha_A \alpha_B \rangle = \langle \alpha_A \alpha_A | \Pi_{ij}^1 | \alpha_A \alpha_A \rangle = \langle \beta_A \beta_B | P_{ij}^2 | \alpha_A \alpha_B \rangle = \langle \beta_A \alpha_A | \Pi_{ij}^1 | \alpha_A \beta_A \rangle = \frac{1}{N}$ , where  $|\alpha\rangle, |\beta\rangle$  denotes two out of  $N$  possible colors of a spin and subscript  $A, B$  denotes different sublattices. In particular, diagonal operators  $P_{ij}^1$  and  $\Pi_{ij}^1$  act only between spins with the same color and make the state intact.  $P_{ij}^2$  paints two spins with the same color into another color,  $|\alpha_A \alpha_B\rangle \rightarrow |\beta_A \beta_B\rangle$  and  $\Pi_{ij}^2$  permutes the colors of two spins with different colors,  $|\alpha_A \beta_A\rangle \rightarrow |\beta_A \alpha_A\rangle$ .

At this stage, we will outline the stochastic series expansion (SSE) QMC sampling process and introduce the generalized loop update for the SU(N) cases. At the start of one MC step, one performs the diagonal update where  $P_{ij}^1$  or  $\Pi_{ij}^1$  is inserted or removed with Metropolis probability determined by the matrix elements listed above. In the next step, linked vertices are constructed to form loops in the configuration. Then, a random color and a starting position are picked. One follows the trajectory of the loop and paints the visited spins with the loop color until the loop closes. An exchange between the diagonal and off-diagonal operators may happen during the painting. Once a loop closes, a new configuration is generated, and one can always accept the update since all the non-zero matrix elements are equal to  $1/N$  and thus share the same weight. Finally, one performs measurements within the new configuration.

Loop moves are designed to avoid zero-weighted configurations for high sampling efficiency. Fig. S1 shows typical vertices that may occur in simulating Hamiltonians with  $P_{ij}$  and  $\Pi_{ij}$ . The upper panel shows the vertices

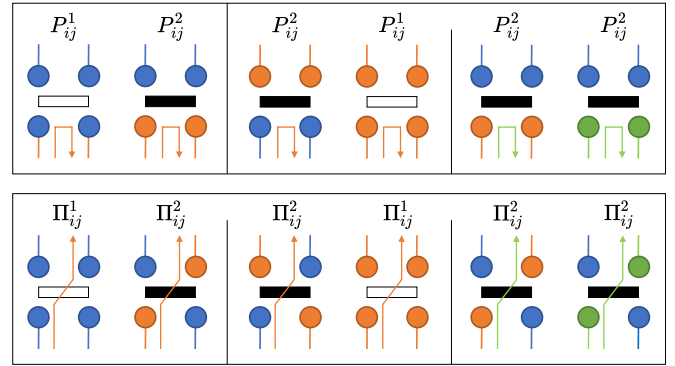


FIG. S1. **Typical vertices of the SU(N) Hamiltonian and different loop updating moves.** The left side of each block is the vertex before the update, and the right side shows the vertex after the update. The upper panel demonstrates the vertices involving nearest-neighbor spin interaction  $P_{ij}$  (switch and reverse move). The lower panel exhibits those for the next-nearest-neighbor interaction  $\Pi_{ij}$  (switch and continue move). Arrows with colors represent the trajectories of colored loops, which paint the spins. Diagonal operator (white bar,  $P_{ij}^1$  and  $\Pi_{ij}^1$ ) and off-diagonal operator (black bar,  $P_{ij}^2$  and  $\Pi_{ij}^2$ ) may transform each other to ensure a non-trivial configuration after the update.

with  $P_{ij}$  requiring a switch and reverse loop move. The lower one shows the vertices with  $\Pi_{ij}$  requiring a switch and continue loop move. The left vertex in each block is before the update, along with the path and color of the loop represented by the colored arrows. The right side of each block illustrates the vertex after the update. The spins visited by the loop are painted with the color of the loop. Meanwhile, the type of the operator is considered to be changed to ensure the new configuration is non-trivial.

## II. INCREMENTAL ALGORITHM FOR THE ENTANGLEMENT ENTROPY COMPUTATION FOR SU(N) SPINS

We implement the recently developed incremental algorithm to compute the EE [31, 59–64] and generalize it to SU(N) spin models. We first parameterize the partition function  $\mathcal{Z}_A^{(2)}$  with  $\lambda$  such that  $\mathcal{Z}_A^{(2)}(\lambda = 0) = \mathcal{Z}_0^{(2)}$  and  $\mathcal{Z}_A^{(2)}(\lambda = 1) = \mathcal{Z}_A^{(2)}$ . More explicitly,  $\mathcal{Z}_A^{(n)}(\lambda) = \sum_{B \subset A} g_A(\lambda, N_B) \mathcal{Z}_B^{(n)}$  where  $B$  is a subset of the entanglement region  $A$ ,  $N_B$  is the number of sites in  $B$  and  $g_A(\lambda, N_B) = \lambda^{N_B} (1 - \lambda)^{N_A - N_B}$  with  $\lambda \in [0, 1]$ . Therefore,  $S_A^{(n)}$  can be written as the integral  $S_A^{(n)} = \frac{1}{1-n} \int_0^1 d\lambda \frac{\partial \ln \mathcal{Z}_A^{(n)}(\lambda)}{\partial \lambda}$  along the path  $\lambda \in [0, 1]$ . Instead of calculating  $e^{-S_A^2}$  directly, we further split this path into  $K$  pieces with a step length  $\Delta$ , the ratio of

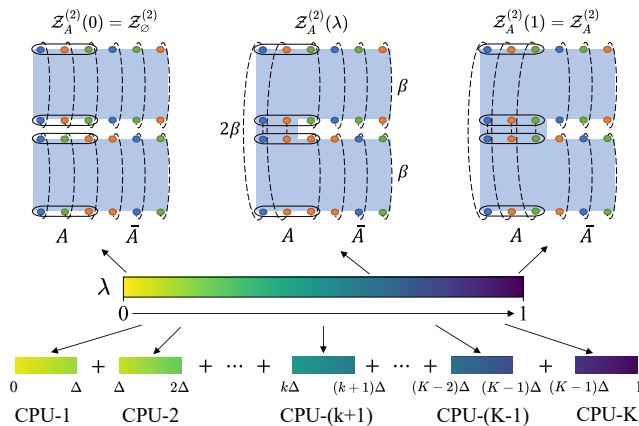


FIG. S2. **The incremental computation of EE.** The entanglement region  $A$  is denoted as the spins inside the circle. As in Eq. (S1), we split the computation of the ratio into the parallel execution of many ratios and compute the EE via a non-equilibrium process characterized by  $\lambda$  evolving from  $\lambda = 0$  to  $\lambda = 1$ . We divide this path into  $K$  pieces and assign each piece to one CPU. The connectivity of spins in  $A$  between two replicas (or topology of the joint partition function) is determined stochastically by  $\lambda$ . As  $\lambda$  increases, more spins in  $A$  from different replicas will be 'glued' together, given that they share the same color, resulting in an imaginary time period of  $2\beta$ . Spins not 'glued' together are in the environment  $\bar{A}$  and experience a regular imaginary time period of  $\beta$ .

partition function can now be written as

$$e^{-S_A^2} = \frac{\mathcal{Z}(1)}{\mathcal{Z}(0)} = \frac{\mathcal{Z}(\Delta)}{\mathcal{Z}(0)} \frac{\mathcal{Z}(2\Delta)}{\mathcal{Z}(\Delta)} \cdots \frac{\mathcal{Z}(k\Delta)}{\mathcal{Z}((k-1)\Delta)} \cdots \frac{\mathcal{Z}(1)}{\mathcal{Z}((K-1)\Delta)}, \quad (\text{S1})$$

where we have suppressed the Rényi index in the intermediate  $\mathcal{Z}$ s on the RHS of Eq. (S1). Each term in the product string, with well-controlled value of  $O(1)$  instead of exponentially small in the LHS of Eq. (S1), is computed in parallel, as shown in Fig. S2. Finally, we multiply these pieces and take a logarithm to get the Rényi entropy  $S_A^2$ .

To implement the algorithm, we first thermalize the regular partition function  $\mathcal{Z}$  and then make two replicas of it as the thermalized configuration of  $\mathcal{Z}_\emptyset^{(2)}$  (the left most configuration in Fig. S2). We divide the interval  $\lambda \in [0, 1]$  into  $K$  pieces with a length of each sub-interval  $\Delta$  and distribute each process to one CPU, as shown in Fig. S2. Take process  $k+1$  as an example,  $\lambda$  evolves from  $\lambda(t_i) = k\Delta$  to  $\lambda(t_f) = (k+1)\Delta$ . At each  $\lambda$  value, we need to determine the topology of  $\mathcal{Z}_A^{(2)}(\lambda)$ . Each site in  $A$  is considered to be 'glued' or 'separated' according to the probability  $P_{\text{join}} = \min\left\{\frac{\lambda}{1-\lambda}, 1\right\}$  and  $P_{\text{leave}} = \min\left\{\frac{1-\lambda}{\lambda}, 1\right\}$ , on condition that spins from two replicas at that site share an identical color. After de-

termining the trace structure, we perform a Monte Carlo update and take measurements. To take non-equilibrium measurements, we gradually increase  $\lambda(t_i) = k\Delta$  by a small value  $h$  and record the value  $\frac{g_A(\lambda(t_{m+1}), N_B(t_m))}{g_A(\lambda(t_m), N_B(t_m))}$ , where  $\lambda(t_m) = k\Delta + mh$ . Each time we increase  $\lambda$ , the topology of  $\mathcal{Z}_A^{(2)}(\lambda)$  should be re-determined. The process is repeated until  $\lambda(t_m) = \lambda(t_f) = (k+1)\Delta$ . At the end of process  $k+1$ , we compute  $\frac{\mathcal{Z}((k+1)\Delta)}{\mathcal{Z}(k\Delta)} = \left\langle \prod_{m=0}^{\Delta/h-1} \frac{g_A(\lambda(t_{m+1}), N_B(t_m))}{g_A(\lambda(t_m), N_B(t_m))} \right\rangle$ . Finally, we multiply the results all processes together to obtain  $S_A^2$  using Eq. (S1).

It is important to note that, although  $e^{-S_A^2(L)}$  is an exponentially small number and therefore exponentially hard to be sampled well as the system size increase, each term on the RHS of Eq. (S1) is of  $O(1)$  and therefore easy to compute precisely [63]. Their product can then be computed accurately, and one then takes its logarithm to obtain the  $S_A^2(L)$ . The divide-and-conquer strategy of the incremental algorithm guarantees the precise determination of the  $S_A^2(L)$  such that one can analyze its finite-size scaling behavior and find the log-coefficient in Eq. (2) in the main text.

### III. STOCHASTIC DATA COLLAPSE

We have devised a method for accurately estimating critical exponents, which involves collapsing data using a stochastic process [64, 113, 114]. This involves fitting a polynomial curve through the data points for various system sizes  $L$ , and the quality of the collapse is determined by how well the data fits the curve. To quantify this, we use the R squared value, denoted by  $R^2$ , representing the variation between the data and the fitted curve. The definition of  $R^2$  is  $R^2 = 1 - \frac{S_{res}}{S_{tot}} = 1 - \delta$ , with  $S_{res} = \sum_{i=1}^n w_i (y_i - \hat{y}_i)^2$ ,  $S_{tot} = \sum_{i=1}^n w_i (y_i - \bar{y})^2$ . The smaller the value of  $\delta$ , or the error of fitting, the better the quality of the collapse.  $S_{res}$  measures the deviation between the actual data and the fitted curve, whereas  $S_{tot}$  measures the variance of the fitted curve itself. The weight  $w_i$  is used to emphasize the importance of the critical region, where the quality of the collapse is of the utmost importance. The  $y$ -value of the scaled data point is denoted by  $\hat{y}_i$ , and that of the fitted curve at the same  $x$ -value is denoted by  $y_i$ . The fitted curve's mean value of all points  $y_i$  is denoted by  $\bar{y}$ .

To investigate the drift of exponents against system sizes, we fix the critical point at the extrapolated value at  $L \rightarrow \infty$  and use three different sizes  $L_{max} - 24, L_{max} - 12, L_{max}$  together at a time to obtain the exponents. Then, we can set  $\beta$  and  $\nu$  as free parameters, and the stochastic process is done in the two-dimensional plane spanned by  $\beta$  and  $\nu$ . A random set of parameters is proposed and fitted by a polynomial curve. Fitting error  $\delta$  is calculated. Then one randomly moves parameters in the

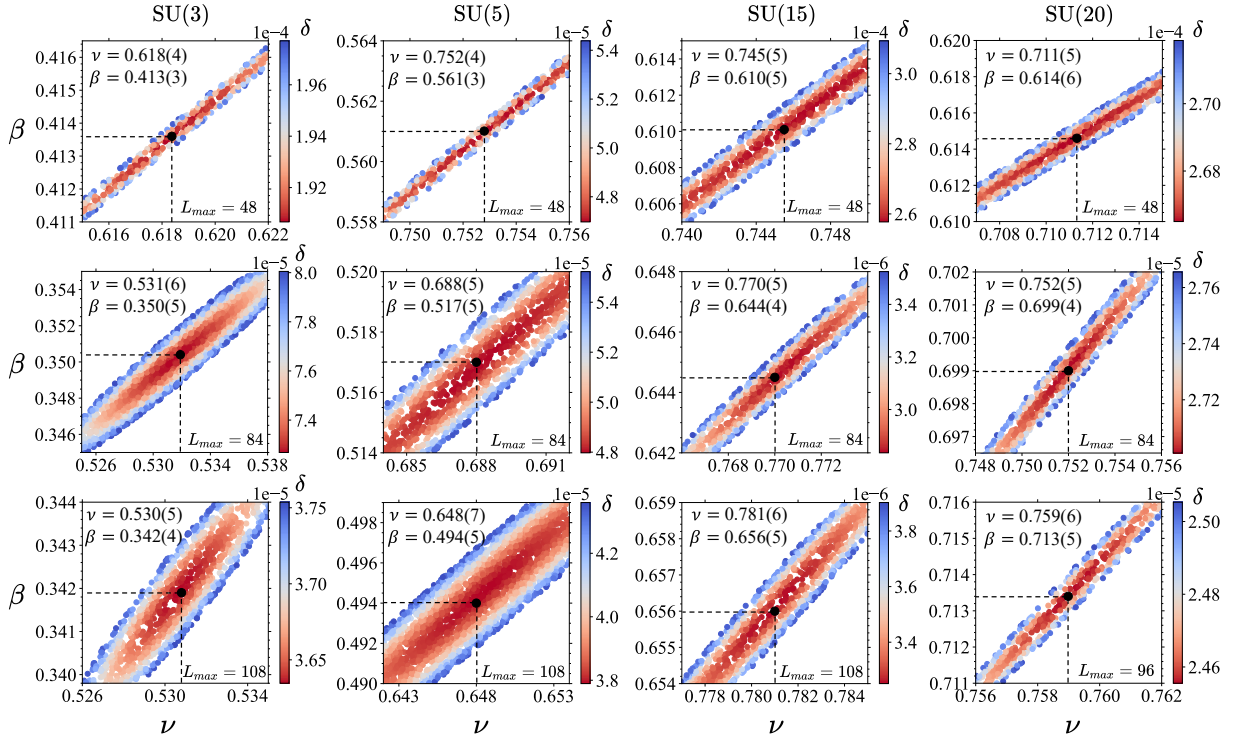


FIG. S3. **Stochastic data collapse to determine critical exponents with different  $L_{max}$ .** Columns display the distribution of fitting error  $\delta$  in the  $\beta - \nu$  plane for SU(3), SU(5), SU(15) and SU(20) respectively with various  $L_{max}$ . Black dots in each panel indicate the optimum sets of exponents in each case.

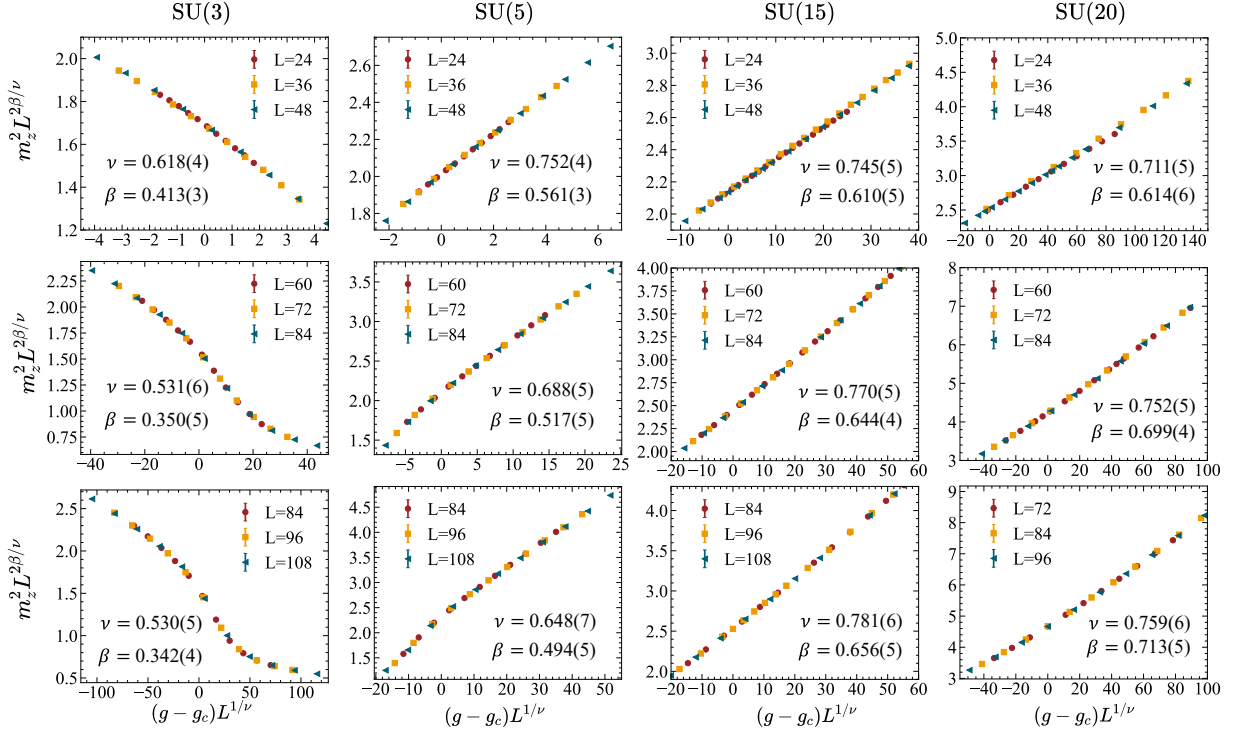


FIG. S4. **Data collapse of squared magnetization of SU(3), SU(5), SU(15) and SU(20) with different  $L_{max}$ .** Each panel shows the data collapse of squared magnetization  $m_z^2$  with three consecutive system sizes  $L_{max} - 24 \sim L_{max}$  using the optimum  $\beta$  and  $\nu$  determined in Fig. S3.



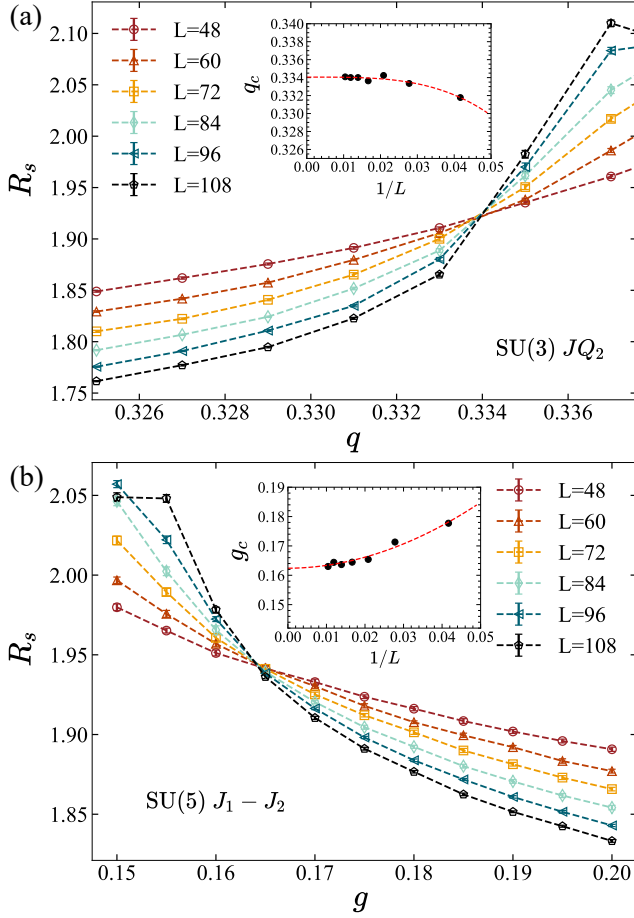


FIG. S5. **Crossing of Binder ratio to determine the  $q_c$  for SU(3) and  $g_c$  for SU(5) cases.** We use the Binder ratio for the antiferromagnetic Néel order to determine the critical  $q = \frac{Q}{J_1+Q}$  for the SU(3) case (panel (a)) and the critical  $g = \frac{J_2}{J_1}$  for the SU(5) case (panel (b)). The simulated system sizes are listed in the legend,  $L = 24, 36, \dots, 72, \dots, 108$ , and  $\beta = L$ . The insets show the extrapolation of the  $q_c$  and  $g_c$  versus  $1/L$ , and our extrapolated critical points are well consistent with those determined in previous literatures [8, 57].

2-d space as shown in Fig. S3 while recording the fitting error  $\delta$ . After enough steps, our best estimation is the parameter set with the smallest error. Distributions of  $\delta$  are exemplified in Fig. S3 for SU(3), SU(5), SU(15) and SU(20) with various  $L_{max}$ . Fig. S4 illustrates the corresponding collapse of squared magnetization  $m_z^2$  using fitted critical exponents  $\nu$  and  $\beta$  in Fig. S3.

#### IV. QMC BENCHMARK OF DQCPs AND DRIFT OF CRITICAL EXPONENTS

In this section, we first show representative data in which the positions of the DQCPs are obtained from the crossing of the Néel order Binder ratios,  $R_s = \frac{\langle m_z^4 \rangle}{(m_z^2)^2}$

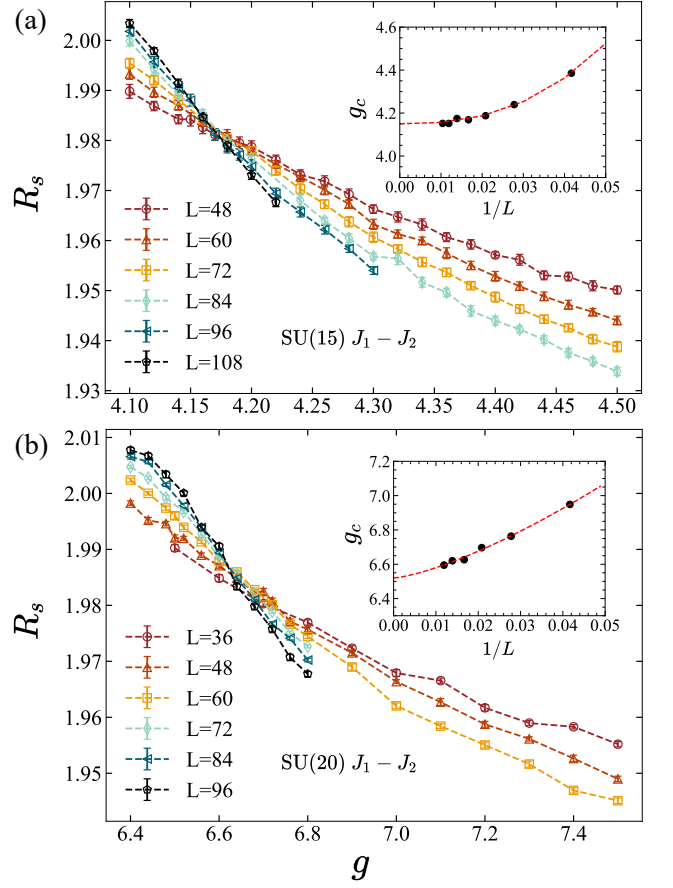


FIG. S6. **Crossing of Binder ratio to determine the  $g_c$  for SU(15) and SU(20) cases.** We use the Binder ratio for the antiferromagnetic Néel order to determine the critical  $g = \frac{J_2}{J_1}$  for the SU(15) (panel (a)) and SU(20) (panel (b)) cases. The simulated system sizes are listed in legends,  $L = 24, 36, \dots, 72, \dots, 108$ , and  $\beta = L$ . The insets show the extrapolation of the  $g_c$  versus  $1/L$ . On these  $g_c$ -s, we performed the entanglement entropy calculation and analysis.

for various SU( $N$ ) cases. For  $N = 3, 5$ , as shown in Fig. S5, our QCP positions are well consistent with previous works [8, 57]. And for  $N = 15, 20$ , as shown in Fig. S6, since no previous data was available, our results of  $g_c$ -s provide the first set of valuable references. The EE computation in the main text is performed upon the  $q_c$ -s and  $g_c$ -s determined in this manner.

Then, we further carry out the finite-size analysis based on stochastic data collapse [64, 113, 114] as introduced in Sec. III to determine the critical exponents as a function of the system size  $L$ , as shown in Fig. S7. Previous work [110] has obtained critical exponents for small  $N = 2, 3, 4$  on the  $J$ - $Q$  model. They found a non-convergent and increasing trend of the exponent  $1/\nu$  against system sizes, implying a first-order transition at  $N = 2, 3, 4$ . Although with relatively smaller system sizes, our estimated exponents,  $1/\nu$  for SU(3) and SU(5) in Fig. S7 manifest a similar non-convergent and increas-

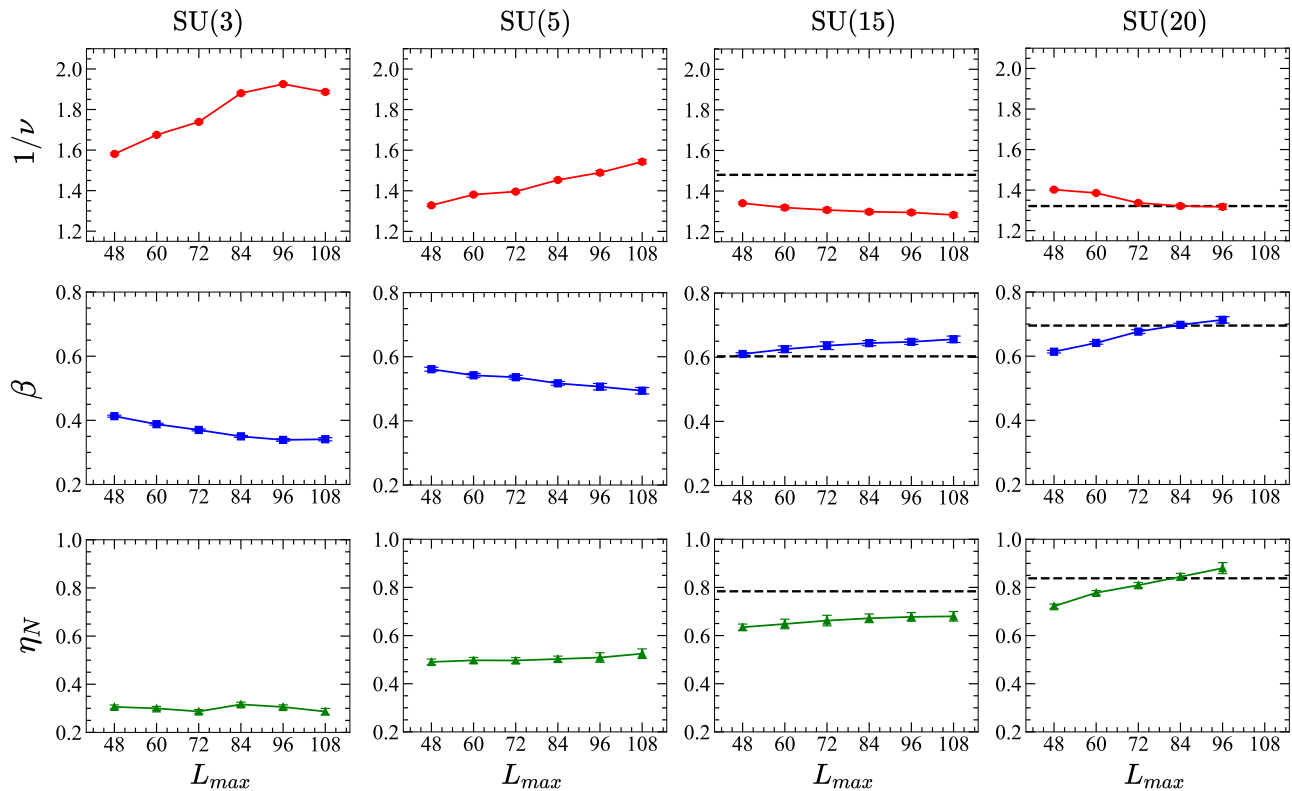


FIG. S7. **Drift of  $1/\nu$ ,  $\beta$  and  $\eta_N$  for SU(3), SU(5) and their convergence in SU(15) and SU(20) cases.** In the cases of the SU(3) and SU(5), one sees  $1/\nu$  values are still not converged as the largest system size  $L_{max}$  used in the stochastic data collapse analysis gradually increases, suggesting that these transitions are weakly-first-order. But in the cases of SU(15) and SU(20), the exponents  $1/\nu$  converge as  $L_{max}$  increases. Dashed lines are the large- $N$  prediction for the AH model:  $\nu^{-1} = (1 - \frac{48}{\pi^2 N})^{-1}$ ,  $\eta_N = 1 - \frac{32}{\pi^2 N}$  and  $\beta = \nu(\eta_N + 1)/2$  at order  $1/N$ .

ing behavior as Ref. [110]. In fact, our estimated exponents for SU(3) match quantitatively well with those in Ref. [110].

On the other hand, when  $N \geq 7$  where the DQCPs are unitary CFTs from the entanglement measurement in the main text, we find in Fig. S7 that for SU(15) and SU(20),  $1/\nu$  values converge quickly against system sizes, showing no anomaly. This observation strengthens our conclusion that  $SU(N < 7)$  transitions are likely to be first-order while  $SU(N \geq 7)$  transitions are continuous and are well described by non-compact  $CP^{(N-1)}$  or AH models.

The last row in Fig. S7 shows our estimated  $\eta_N =$

$2\beta/\nu - 1$  for the antiferromagnetic order. It is interesting to see that, in the SU(3) case, our  $\eta \sim 0.3$  and in the SU(5) case, our  $\eta \sim 0.5$ , are all consistent with previous values [55] upto the system sizes we study. Moreover, the dashed lines in Fig. S7 indicate the large- $N$  prediction for the AH model:  $\nu^{-1} = (1 - \frac{48}{\pi^2 N})^{-1}$  and  $\eta_N = 1 - \frac{32}{\pi^2 N}$  at order  $1/N$  [39, 66]. Our obtained  $1/\nu$  and  $\eta_N$  values at  $N = 15, 20$  follows the trend of large- $N$  prediction. As  $N$  becomes larger, our numerical result gradually approaches the theoretical prediction, manifesting the vanishing of higher order corrections at large enough  $N$ . Our SU(20) result matches the large- $N$  AH model prediction quantitatively, providing precious results in addition to those reported in Ref. [57].